

# ADVANCED MATERIALS

## Supporting Information

for *Adv. Mater.*, DOI: 10.1002/adma.201204055

**Design of Battery Electrodes with Dual-Scale Porosity to  
Minimize Tortuosity and Maximize Performance**

*Chang-Jun Bae, Can K. Erdonmez, John W. Halloran, and  
Yet-Ming Chiang\**

## SUPPORTING INFORMATION

### Section 1 – Theory for tortuosity reduction at fixed total porosity using array of straight channels

Consider an electrode of fixed thickness,  $T$ , overall porosity,  $P$ , composed of a fixed active material and free of binders and conductive additives. Channel spacing,  $\lambda$ , and the relative allocations of total porosity into channels and distributed porosity in the surrounding matrix are the degrees of freedom that define the design.

Now, consider two limiting cases of behavior, compared to the reference case of a porous electrode with homogenous porosity (*i.e. free of channels*). In the first limiting case, channels are present, but negligible net transport occurs along them due to ineffective design of the channel array. In the second case, ion transport through the channels is efficient and dominates the overall ionic transport. For each of these limiting cases, the maximum concentration difference across any two points in the electrode is determined and compared to the concentration difference across the homogenous, reference electrode of the same overall porosity. The magnitude of the concentration drop provides a measure of the effective overall tortuosity of the electrode design – the larger the concentration drop across the electrode at steady state, the higher the effective tortuosity for ion transport across the electrode.

The estimation of the concentration drop for the various cases is based on a steady-state picture as described by Doyle and Newman.<sup>[4]</sup> We further simplify the discussion by ignoring the role of the separator. See Fig. 1A for a description of the geometry under consideration.

**Reference Case – Homogenous electrode, 1D transport:** We modify Doyle and Newman’s assumptions in the following ways: 1) assume that the Bruggeman dependence of the tortuosity on porosity also contains a constant pre-factor,  $\gamma$ , 2) take the limit of the separator thickness going to zero, 3) ignore terms containing the transference number as they do not vary between the cases considered. With those modifications, Doyle and Newman’s Eqn. 21 simplifies to:

$$i_L = \frac{6FD_0C_0P^{3/2}}{T\gamma} \quad (S1)$$

where  $i_L$  is the limiting current density,  $C_0$  the initial electrolyte concentration,  $F$  the Faraday constant,  $D_0$  the diffusion coefficient in the free electrolyte and  $P$  the electrode porosity. We focus, not on the minimum value of the concentration ( $C = 0$  locally at depletion) as Doyle and Newman did, but rather on the magnitude of the concentration drop across the electrode,  $\Delta C$ . In this case, given the parabolic concentration profile and the invariance of the spatial average of the electrolyte concentration between the operating and resting states, the total concentration difference is simply three times the difference between the initial homogenous electrolyte concentration and the minimum concentration. Now, we can generalize the relationship between the concentration drop and the current density,  $i$ , to all  $i < i_L$  as follows:

$$\Delta C_H = \left[ \frac{\gamma T}{2FD_0P^{3/2}} \right] i \quad (S2)$$

where subscript H denotes the homogenous electrode.

**Limiting Case 1 – 1D Transport through Matrix:** Due to a combination of small channel diameter and/or “large” channel spacing, only a limited amount of material around the channel may be accessible by electrolyte diffusion within the timescale of discharge. In that case, further away from the channel, one-dimensional transport parallel to the channels across the matrix dominates. The steady-state concentration drop in this case is modified from the previous expression to account for the constraint of fixed *overall* porosity. Due to allocation of some porosity to the “ineffective” channels,

the matrix porosity is assumed a lower value, given by  $(P - P_C)/(1 - P_C)$ , where  $P_C$  is the porosity that can be attributed solely to channels. Additionally, matrix tortuosity increases correspondingly according to  $\tau = \gamma \varepsilon^{-0.5}$ . These effects result in a concentration drop,  $\Delta C_{1D}$ , across the electrode (far from the sparse/narrow channels):

$$\frac{\Delta C_{1D}}{\Delta C_H} = \left[ \frac{1 - P_C}{1 - (P_C/P)} \right]^{\frac{3}{2}} \quad (S3)$$

For  $P_C \rightarrow 0$ ,  $\Delta C_{1D}$  tends to  $\Delta C_H$ . On the other hand, for  $P_C \rightarrow P$ ,  $\Delta C_{1D}$  diverges as expected due to vanishing porosity in the matrix. In the latter case, transport through this path becomes negligible, given its diverging resistance.

**Limiting Case 2 –Diffusion Axially along Channels & Radially into Matrix:** Now consider ion diffusion inside the cylindrical cell depicted in Fig. 1 in the case that transport along the channel array dominates over the alternative pathway described in the previous case. We construct an upper bound for the concentration drop across the electrode assuming all transport passing through the channel before diffusing laterally into the surrounding matrix. This value is estimated as  $\Delta C_{CH} + \Delta C_L$  where subscript CH corresponds to the expression obtained by considering transport only along the channel; subscript L corresponds to the expression obtained by considering only lateral (i.e. radial) diffusion in the surrounding shell of matrix material. Effectively, we make the approximation that  $Li^+$  ions travelling from the counter electrode to point  $\beta$  (see Figure 1A), travel first along the channel to the end of the channel and then travel laterally across the matrix .

Given the blocking current collector at the electrode base, the same parabolic form for the concentration along position is obtained along the channel as was also seen in the reference case and the first limiting case. The differences are that: 1) for the liquid-filled channel, porosity and tortuosity both equal unity, 2) the sink term that dictates the curvature of the concentration profile has a different value, as there is no net uptake of ions inside the channel. Assuming that the surrounding matrix acts as an efficient, uniform sink along the channel length, uniform local ion uptake of  $j = I/(FV)$  may be assumed along the channel, with  $I$  the total current across the unit cell and  $V$  the volume of the electrolyte-filled channel. For 1D, steady state diffusion with vanishing flux at one boundary, the concentration drop is,

$$\Delta C_{CH} = \frac{j T^2}{2 D_0} \quad (S4)$$

Substituting  $I = i\pi R^2$  and that  $V = \pi T P_C R^2$  (with  $R$  the radius for the cylindrical unit cell) into the expression for  $j$ , we find that,

$$\frac{\Delta C_{CH}}{\Delta C_H} = \frac{\sqrt{P}}{\gamma(P_C/P)} \quad (S5)$$

For radial or lateral diffusion into the matrix from the channel. we estimate the ion concentration drop in the following way. First, consider steady-state diffusion in a cylindrical geometry, with the radial coordinate denoted  $r$ . Radial flux on the unit cell wall, at  $r = R$ , vanishes by (approximate) translational symmetry. Then, the concentration difference between the channel boundary (at  $= R\sqrt{P_C}$ ) and the cell wall can be written as

$$\Delta C_L = \frac{j R^2}{4 D} [P_C + \ln(1/P_C) - 1] \quad (S6)$$

with effective diffusion constant  $D = \gamma^{-1} D \varepsilon_M^{3/2}$ . As before, local porosity in the matrix,  $\varepsilon_M = (P - P_C)/(1 - P_C)$  and  $j = (i\pi R^2)/(FV)$ , but now with uptake volume  $V$  equaling the volume of the matrix material,  $V = \pi T(1 - P_C)R^2$ . Also, for maintaining unit cell volume when approximating the

hexagonal cell by a cylindrical one,  $R \cong \lambda/1.9$  with  $\lambda$  the channel spacing in the array (see Figure 1). Combining the equations in this paragraph and substituting into Equation S6, we find that,

$$\frac{\Delta C_L}{\Delta C_H} \approx \left[ \frac{\lambda}{2.7 T} \right]^2 \times [P_C + \ln(1/P_C) - 1] \times \sqrt{\frac{1 - P_C}{[1 - (P_C/P)]^3}} \quad (S7)$$

**Limiting Behaviors of Electrode as a Function of Design Parameters:** In a design where the major bulk of ion transport passes through the engineered channels, radial diffusion across the matrix and axial diffusion along the channels can be considered to be processes in series. Diffusion parallel to the channels inside the matrix, on the other hand is a parallel process. To definitively address the question of whether a dual-porosity distribution can lead to improved transport, we first construct an upper bound for the concentration drop across the electrode, under the conservative assumption of the faster path “short-circuiting” the slower path. In that case, the overall concentration drop is,

$$\Delta C = \min (\Delta C_{1D}, \Delta C_{CH} + \Delta C_L) \quad (S8)$$

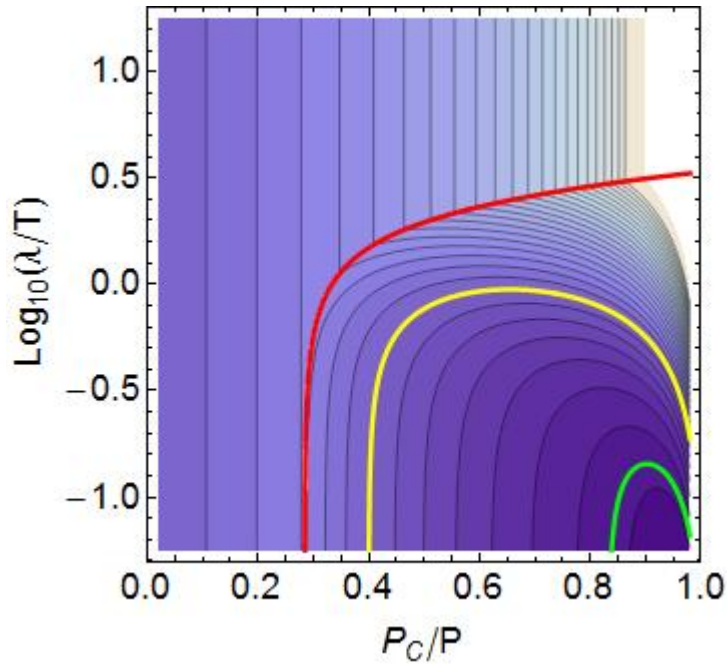
Using this form corresponds to assuming that only the path with the lower concentration drop (i.e. lower resistance) operates, with the minor path being completely bypassed. Together with the constrained transport path we assume, this form overestimates the steady state concentration when both paths contribute (as they usually do, to varying relative degrees), and matches the steady state drop exactly in limiting cases. Equation S8 is used in this section to establish definitive upper bounds on electrode performance; in the next section, an alternate “addition rule” is presented and used to construct the results shown in the main text.

Figure S1 below shows a contour plot of  $\Delta C/\Delta C_H$  as described by Equations S8, S3, S5 & S7. Here, we show the case for  $P = 0.36$ , which roughly corresponds to the experimental samples prepared. We assumed  $\gamma = 1.5$  as described in the text. We arrive at the independent variables for the plot by inspection of the common forms in Eqn.s S3, S5 & S7; they were chosen to be  $\log_{10}(\lambda/T)$  and  $(P_C/P)$ . The bold red line marks where the two limiting paths have the same concentration drop associated with them, *i.e.*  $\Delta C_{1D} = (\Delta C_{CH} + \Delta C_L)$ . Above and to the left of this line,  $\Delta C_{1D} < (\Delta C_{CH} + \Delta C_L)$  and 1D transport inside the homogenous matrix contributes more significantly than transport along channels. Below and to the right of the line, transport along channels dominates. Given the form assumed in Equation S8, it is not surprising that, in this plot,  $(\Delta C/\Delta C_H)$ , assumes the form of two distinct branches joined at the boundary marked by the red line.

A number of features are apparent in Figure S1 whose generalizations to arbitrary  $P$  and  $\gamma$  are apparent. Firstly, the lowest values of  $\Delta C/\Delta C_H$  are achieved in the low right corner of the plot, *i.e.* in the limit  $(V_{CH}/V_P) \rightarrow 1, (\lambda/T) \rightarrow 0$ . This makes sense physically, as this corresponds to the case of vanishingly fine walls of active material surrounding perfectly straight channels. In this limit,  $\Delta C_{1D} \gg \Delta C_{CH} \gg \Delta C_L$ ; thus, the overall concentration drop is the drop across a channel, given by Equation S5, with  $P_C = P$ :

$$\left[ \frac{\Delta C}{\Delta C_H} \right]_{min} = \frac{\sqrt{P}}{\gamma} \quad (S9)$$

The achievement of this minimum concentration is equivalent to building a homogenous electrode of tortuosity of one; rederiving Equation S2 under the assumption  $\tau = 1$  would yield a value for  $\Delta C_H$  reduced by precisely the same factor as the right hand side of Equation S9.



**Figure S1** - Contour plot of *upper bound* for concentration drop across electrode of engineered porosity, normalized by the concentration drop across homogenous electrode of same overall porosity. Overall porosity is fixed at 0.36 and the prefactor in the modified Bruggeman relationship,  $\gamma$ , is taken to be 1.5. See text for details.

The other limiting behaviors of the expression are also reasonable. Either as  $P_C \rightarrow 0$  or as  $\lambda \gg T$ ,  $\Delta C \rightarrow \Delta C_{1D}$ . In the former case, the concentration drop across the electrode approaches the value for the homogenous electrode as the volume devoted to channels becomes negligible. In the latter case, channels, while comprising a measurable and perhaps large fraction of total porous volume, are separated by too large a distance and we find that  $\Delta C > \Delta C_H$ , i.e. introduction of channels while keeping overall porosity constant is predicted to degrade rate performance due to increased tortuosity and reduced porosity of the matrix that is not well-supplied widely spaced channels.

The bold yellow line in Figure S1 marks  $\Delta C = \Delta C_H$ ; inside this contour, there is improved transport over the homogenous case. Considering the conservative manner in which we have approximated  $\Delta C$  so far, a minimum value of  $(P_C/P)$  and a high “resolution” ( $\lambda \lesssim T/2$ ) achieved simultaneously appear to guarantee rate performance improvements upon introduction of the channel array. The shapes of the contours reveal in general that, at fixed  $\lambda/T$ , there is an optimum value of  $(P_C/P)$ , corresponding to a relative channel diameter, that minimizes concentration drop across the structure and maximizes rate performance.

Finally, the green bold line shows  $\Delta C = 1.2 \Delta C_{Min}$ . Inside that contour, the concentration drop across the electrode is at most 20% higher than the minimum achievable value, which also represents a factor of 2 reduction in concentration drop over the reference case. This appears to be achievable with  $T/\lambda > 10$  and  $P_C > 0.85P$ . Note that the co-extruded structures described in the main text have  $T/\lambda$  as high as 13; therefore, it seems reasonable in the future to pursue electrodes with higher matrix density and/or larger relative channel diameter.

**Between the Limiting Cases:** The simple model, described in the previous paragraphs displays correct behavior in various limiting cases. However, due to the conservative nature of Equation S8, it significantly overestimates the concentration drop across the electrode when  $\Delta C_{1D} \approx \Delta C_{CH} + \Delta C_L$ . If we instead assume that fluxes along each major path (radially across the active material and along the channel axis *versus* across the matrix) add independently, we obtain an alternate form mimicking the addition of parallel resistors:

$$\Delta C = \left[ \frac{1}{\Delta C_{CH} + \Delta C_L} + \frac{1}{\Delta C_{1D}} \right]^{-1} \quad (\text{S10})$$


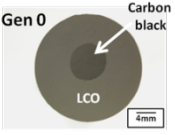
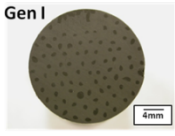
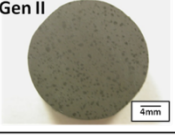
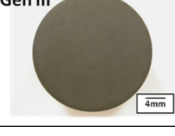
This form has the virtue of smoothly interpolating between the two disjoint branches of Equation S8 while tending to the same behavior far from  $\Delta C_{1D} \approx \Delta C_{CH} + \Delta C_L$ . We use the parallel addition to rule to construct Fig. 1B and Fig. 1C in the main text as it better illustrates the likely behavior of the electrodes in the transition between limiting regimes. The figures are explained in the text; their construction follows the treatment outlined here, with the rule in Equation S10 applied in place of Equation S8.

**Obtaining the Effective Tortuosity for Electrode:** To translate these calculations into an overall effective tortuosity for the electrode design containing channels, we compute the tortuosity of a homogenous reference that would produce an identical concentration drop. This allows us to convert the concentration drop estimated by Equation S10 to an estimate of *the effective tortuosity of the engineered electrode under steady-state discharge*. The equation that allows us to do that is simple:

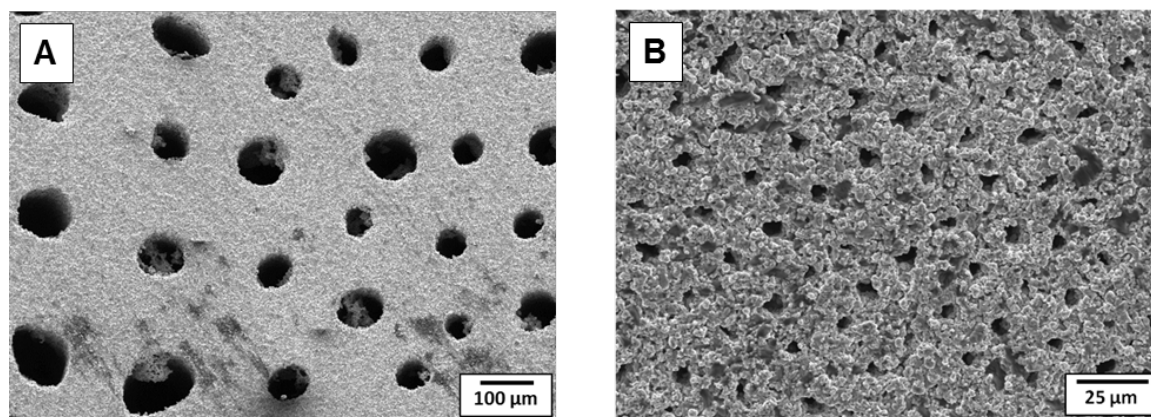
$$\tau_{eff} = \frac{[\Delta C / \Delta C_H]}{[\Delta C / \Delta C_H]_{min}} = \frac{\gamma}{\sqrt{P}} \left[ \frac{\Delta C}{\Delta C_H} \right] \quad (\text{S11})$$

That is, we multiply the normalized concentrations by  $\gamma/\sqrt{P}$ . This has been done in Figs. 1B and 1C in the main text.

## Section 2 – Design of co-extruded samples

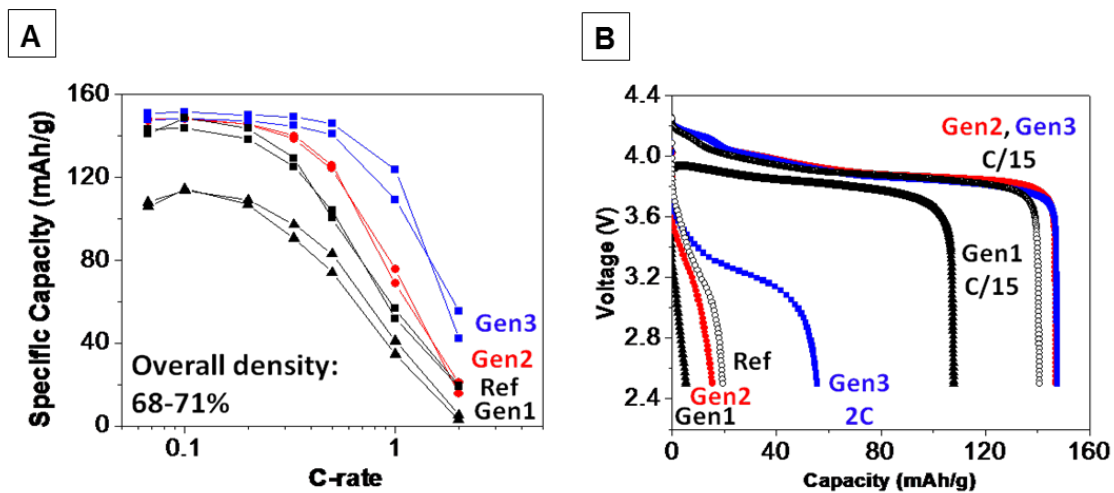
Reduction factor	Extrusion Generation	Image	Unit cell size	Pore size = Carbon black	Channel distance
 $1/11^1$  $1/11^2$  $1/11^3$	0		22000 $\mu\text{m}$	7500 $\mu\text{m}$	
	1		2000 $\mu\text{m}$	680 $\mu\text{m}$	1320 $\mu\text{m}$
	2		180 $\mu\text{m}$	60 $\mu\text{m}$	120 $\mu\text{m}$
	3		17 $\mu\text{m}$	6 $\mu\text{m}$	11 $\mu\text{m}$

**Table S1.** Overall dimensions of co-extruded green body samples, Gens 0-3, based on 11-fold size reduction each extrusion, before sintering.



**Figure S2.** Top section of sintered  $\text{LiCoO}_2$  cathode electrodes, A) Gen 2 and B) Gen 3. In Gen 2, the channel diameters and distances observed match predictions based on the process design summarized in Table S1 but some channels noticeably larger than 60  $\mu\text{m}$  in diameter are also visible. In Gen 3, the additional co-extrusion process has yielded much finer and more closely spaced channels.

Section 3 – Test Results for 70% Dense Sample



**Figure S3.** A) Specific capacity vs. discharge rate and, B) voltage vs. discharge capacity for electrodes with overall density of 70%, compared to a homogeneously porous reference sample. Sample specifications are given in Table S1.